polysaccharides

MDPI

Article

Sequential Oxidation on Wood and Its Application in Pb^{2+} Removal from Contaminated Water

Priyanka R. Sharma *, Sunil K. Sharma, Marc Nolan, Wenqi Li, Lakshta Kundal and Benjamin S. Hsiao *

Chemistry Department, Stony Brook University, John S. Toll Drive, Stony Brook, NY 11794, USA; sunil.k.sharma@stonybrook.edu (S.K.S.); marc.nolan57@gmail.com (M.N.); wenqi.li7@gmail.com (W.L.); lakshta.kundal@stonybrook.edu (L.K.)

* Correspondence: priyanka.r.sharma@stonybrook.edu (P.R.S.); benjamin.hsiao@stonybrook.edu (B.S.H.); Tel.: +1-6315423506 (P.R.S.); +1-6316327793 (B.S.H.)

Abstract: Raw wood was subjected to sequential oxidation to produce 2,3,6-tricarboxycellulose (TCC) nanofibers with a high surficial charge of 1.14 mmol/g in the form of carboxylate groups. Three oxidation steps, including nitro-oxidation, periodate, and sodium chlorite oxidation, were successfully applied to generate TCC nanofibers from raw wood. The morphology of extracted TCC nanofibers measured using TEM and AFM indicated the average length, width, and thickness were in the range of 750 ± 110, 4.5 ± 1.8, and 1.23 nm, respectively. Due to high negative surficial charges on TCC, it was studied for its absorption capabilities against Pb^{2+} ions. The remediation results indicated that a low concentration of TCC nanofibers (0.02 wt%) was able to remove a wide range of Pb^{2+} ion impurities from 5–250 ppm with an efficiency between 709–99%, whereby the maximum adsorption capacity (Q_m) was 1569 mg/g with R^2 0.69531 calculated from Langmuir fitting. It was observed that the high adsorption capacity of TCC nanofibers was due to the collective effect of adsorption and precipitation confirmed by the FTIR and SEM/EDS analysis. The high carboxylate content and fiber morphology of TCC has enabled it as an excellent substrate to remove Pb^{2+} ions impurities.

Keywords: tricarboxycellulose; oxidized cellulose; wood; 6-carboxycellulose; adsorption

Citation: Sharma, P.R.; Sharma, S.K.; Nolan, M.; Li, W.; Kundal, L.; Hsiao, B.S. Sequential Oxidation on Wood and Its Application in Pb^{2+} Removal from Contaminated Water. *Polysaccharides* **2021**, *2*, 245–256. https://doi.org/10.3390/polysaccharides2020017

Academic Editor: Hyun Chan Kim

Received: 1 January 2021
Accepted: 29 March 2021
Published: 7 April 2021

1. Introduction

Cellulose is a naturally occurring, renewable, inexpensive, and environmentally friendly material that exhibits properties that make it a viable biomaterial [1]. It is the most abundant biopolymer on Earth, and approximately 1.5 trillion tons of cellulose biomass are produced on an annual basis [2]. It is comprised of β-(1-4)-linked D-glucose units and are linked at the C1 and C4 positions of the anhydroglucose units (AGUs). The most active groups are the hydroxyl groups (-OH) that appear at the C2, C3, and C6 positions. Oxidation of these hydroxyl groups into carboxyl groups can modify the properties of cellulose and generate an important derivative of cellulose called carboxycellulose [3].

Research studies have been conducted to find environmentally friendly, low-cost, and low energy means of extracting carboxycellulose from biomasses that will replace synthetic polymers in applications. Carboxycellulose is known to be used in a wide range of applications such as orthopedics, textiles, biomedical, water purification, wound dressings, food packaging, among many others [4–7]. When carboxycellulose fibers are extracted in nanoscale ranges (e.g., nanofibers (L ≥ 1000 nm, W ≥ 10 nm), nanocrystals (L ≥ 500 nm, W ≥ 100 nm)), these nanoscale fibers appear with advanced properties such as an increase in surface area, improvement in dispersion, good aspect ratio, etc., which enabled its utility in high tech applications such as water purification [8–13], nanocomposites [14,15], drug delivery [16], lightweight foams and aerogels [17], and biomaterials [9,18,19]. Carboxycellulose can be differentiated into three derivatives: (1) 6CC: 6-carboxycellulose, where the C6 position of anhydroglucose unit of cellulose possess carboxyl group. This is mostly produced by TEMPO-oxidation [20] and nitro-oxidation [3,9] methods. (2) DCC:

dicarboxycellulose, where the C2 and C3 positions of anhydroglucose unit of cellulose consist of carboxyl groups. This is produced by the sodium chlorite oxidation on 2,3-dialdehyde cellulose (DAC) produce by sodium periodate oxidation [21,22]. (3) TCC; 2,3,6-tricarboxycellulose where the C2, C3, C6 positions of anhydroglucose units of cellulose oxidize to carboxyl groups [23–25]. When these carboxyl groups present in ionic forms (carboxylate (COO^-) group), this assists in the dispersion of nanofibers in the suspensions phase and provides the active functional sites that can be utilized for niche applications including fluorescent labeling [26], biosensors [27], and metal ion remediation [28].

In this study, we have introduced raw wood to produce 6CC using the nitro-oxidation method. In previous studies, the nitro-oxidation method was performed on softwood and grasses [3,8,29] to produce 6CC nanofibers. Nitro-oxidation is a simple, less-chemically oriented, and cost-effective pathway as compared to TEMPO-oxidation to generate 6CC nanofibers. Hence, we have utilized this method to produce highly charged TCC from raw wood. The whole process of producing TCC from raw wood involve sequential oxidation using (i) nitro-oxidation; (ii) periodate oxidation, and (iii) sodium chlorite oxidation.

TCC nanofibers have been used widely in biomedical applications such as in surgical gauzes [30], wound dressing materials [31], hemostatic material [32], drug delivery [33,34], lanthanum recovery [35], and antibacterial and antituberculosis material [36]. Spherical-shape TCC nanoparticles are also discussed in the literature and used to stabilize carbon nanotubes suspension with minimal ultrasonication [37–39]. There have been few reports dealing with the successful selective oxidation of TCC nanofibers that have been carried out in a simple and cost-effective manner. It has been previously studied [28] that the adsorption of heavy metal ions by the carboxycellulose nanofibers increases with higher carboxylate concentrations. However, previous studies have only shown high concentrations of carboxylate groups in 6CC nanofibers. This study looks to produce TCC nanofibers, which we have hypothesized will lead to a higher concentration of carboxylate groups than the 6CC nanofibers because, in TCC, all three active hydroxyl groups will randomly transform to carboxylate groups (COO^-) or ionic sites. Additionally, in TCC, the original AGU structure will be disturbed due to breakage of C2 and C3 bond that will cause a reduction in crystallinity of nanofibers. Hence, we assume that the increase in carboxylate content and reduction in crystallinity in TCC will increase the adsorption properties of TCC, making it a more effective adsorbent.

2. Materials and Methods

Raw wood was purchased from Brinkmann (Hickory Wood Chips, New York, NY, USA), which was purchased at local hardware stores. The wood chips were first cut into small pieces (less than 2 cm) and then put into an IKA MF10 basic grinder to be turned into a fine powder (200 µ). The samples were not washed nor subjected to any pretreatments or bleaching processes before the reactions.

2.1. Preparation of 6CC Using Nitro-Oxidation

The 6CC fibers were prepared following the procedure described in Sharma et al., 2017 [9]. In accordance with this procedure, 10 g of untreated fibers was placed in a three-necked, round-bottom flask (RBF), and then 140 mL of 60% nitric acid was added into it and allowed to spin via stir bar and magnetic stirrer. After 20 min, 9.6 g of sodium nitrite was added to the mixture and the reaction could take place for 12 h at 50 °C. After 12 h, the reaction was stopped by adding 250 mL of distilled water to the solution. The reaction mixture was then poured into the beaker. The fibers settled at the bottom of the beaker after a few minutes, and the upper portion (liquid) was decanted into a separate beaker, which was then neutralized with sodium bicarbonate. The process of decantation was repeated 3–4 times. Then, the fiber slurry was put into a dialysis bag and kept in distilled water for further purification. The conductivity of the water was continually checked for two weeks until the conductivity was under 5 µS. Once the conductivity reached below 5 µS, preparation of DAC could begin.

2.2. Preparation of 2,3-dialdehyde Using Sodium Metaperiodate Oxidation

Following the dialysis of the 6CC fibers, the procedure from Varma, 2002 [22] was followed to produce DAC; however, certain parameters were modified to suit the current study. More specifically, a 100 mL suspension of water containing approximately 1.0 g 6CC fibers was added to a 250 mL glass bottle. The bottle was first wrapped in aluminum foil to prevent the exposure of light, and the lights were turned off to decrease any potential light exposure. Then, 0.5 g of sodium metaperiodate was added to the bottle, and the reaction was continued for 6 h in an oil bath kept at 52 °C with the lights turned off so as not to expose the samples to light, and was continuously stirred via a stir bar. After 6 h, the reaction was quenched by adding 50 mL of ethanol and allowed to stir for another 15 min. The samples were then put into dialysis bags for purification, and the conductivity was monitored. The sample was put through the centrifuge multiple times at 5000 rpm for 15 min until the upper suspension of the solution had a pH of 7.

2.3. Preparation of TCC Using Sodium Chlorite Oxidation

Following the production and centrifugation of the DAC fibers, the sample (6-carboxy-2,3-dialdehyde cellulose) was subjected to sodium chlorite oxidation to produce TCC fibers. More specifically, approximately 0.5 g of the sample (in suspension) was placed into a 600 mL beaker. Then, a measured amount of sodium chlorite (0.838 g) and acetic acid (0.278 mL) was dispersed in 50 mL of water and then added slowly, dropwise, into the 6-carboxy-2,3-dialdehyde cellulose suspension. The reaction was carried out for 6 h between 20–25 °C and constant stirring via stir bar. After 6 h, the reaction was quenched with 100 mL of ethanol. The solution was then washed with ethanol and centrifuged four times each at 6000 rpm for 10 min. The scheme for the preparation of TCC is presented in Supplementary Information in Figure S4.

The structural and functional characterization of 6CC and TCC was performed using Fourier transform infrared spectrometer (FTIR) (PerkinElmer Spectrum One instrument, Melville, NY, USA) in attenuated total reflectance (ATR) mode, ^{13}C CPMAS NMR (Bruker Utrashield 500 WB plus (500 MHz) NMR instrument), and wide-angle X-ray diffraction (WAXD) (Benchtop Rigaku MiniFlex 600, Rigaku Corporation, Wilmington, MA, USA). The morphology of 6CC and TCC was analyzed by transmission electron microscopy (TEM) (FEI Tecnai G2 Spirit BioTWIN instrument, Hillsboro, OR, USA), atomic force microscopy (AFM) (Bruker Dimension ICON scanning probe microscope, Bruker Corporation, New York, NY, USA), and scanning electron microscopy (SEM/EDS) (Zeiss LEO 1550 SFEG-SEM instrument, New York, NY, USA).

2.4. Preparation of Pb^{2+} Solution for Removal Study

A stock solution of 5000 ppm $Pb(OAc)_2$ (lead (II) acetate) contaminated water was made by dissolving 0.4795 g of $Pb(OAc)_2$ in 50 mL of H_2O. A serial dilution was then carried out to obtain solutions with the following concentrations (in ppm): 250, 100, 50, 25, 10, and 5. For the remediation experiments, 5 mL of each concentrated lead (II) acetate solution was mixed with 5 mL of the 6CC nanofibers. The same parameters were followed for remediation experiments with the TCC nanofiber solutions. Each nanofiber solution had a wt% of 0.02.

2.5. Static Adsorption Study

The static adsorption study on Pb^{2+} and TCC was performed by employing the data obtained from ICP-MS analysis. The data obtained were used to calculate Qe (adsorption capacity adsorbed at equilibrium) and plotted against Ce (equilibrium concentration of adsorbate). The ICP-MS data was evaluated using Langmuir Isotherm model. Langmuir

model is based on monolayer adsorption on the active site of adsorbent, Langmuir isotherm model is expressed in Equation (1):

$$\frac{Ce}{Qe} = \frac{Ce}{Qm} + \frac{1}{QmK} \quad (1)$$

where: Ce-equilibrium concentration of adsorbate; Qe-adsorption capacity adsorbed at equilibrium; Qm and K-Langmuir constants which can be calculated from the intercept and slope of the linear plot based on Ce/Qe versus Ce [40].

3. Results and Discussion

3.1. Structural Characterization of 6CC and TCC

Figure 1 shows the structure of 6CC and TCC. The structure of 6CC possesses repeated anhydroglucoronic units with carboxylic (COOH) or carboxylate (COONa) groups distributed randomly at C6 carbon. While TCC structure shows repeated anhydroglucoronic units with carboxylic (COOH) or carboxylate (COONa) groups presented arbitrarily at C6, C2, C3 carbons.

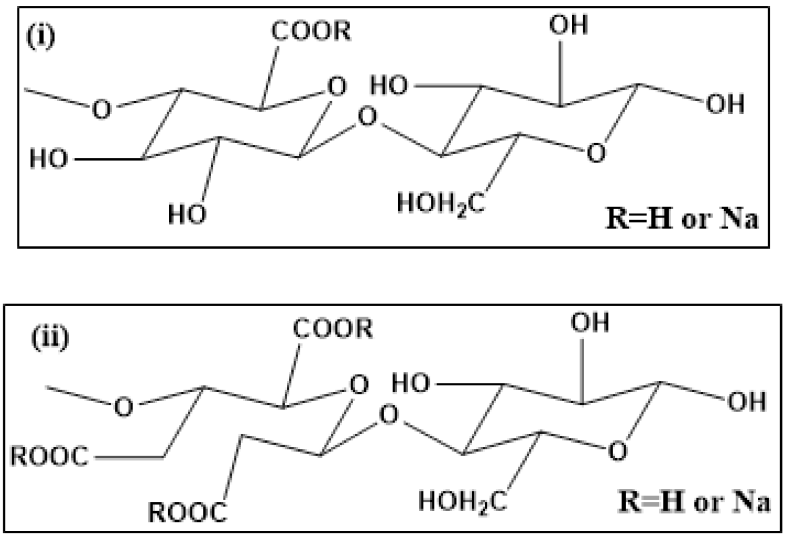

Figure 1. Structure of (**i**) 6CC, (**ii**) TCC.

The FTIR spectra of raw wood in Figure 2i shows several characteristic peaks whereby 3328 cm^{-1} corresponded to OH stretching and peaks at 2900 cm^{-1} belonged to C–H symetrical stretching in the cellulose unit; 1515 cm^{-1} was responsible for C=C aromatic symmetrical stretching in the lignin unit; 1739 cm^{-1}, 1460 cm^{-1}, 1240 $cm^{-1,}$ and 810 cm^{-1} resembled to xylan and glucomannan of hemicellulose moieties. It was observed that the OH stretching peak at 3328 cm^{-1} in 6CC and TCC became much sharper than that in raw wood. This could be due to the disturbance in the hydrogen bonding from the modification of C6 primary hydroxyl groups to carboxyl groups in anhydroglucose units of the cellulose chain. Notably, the peak at 1597 cm^{-1} appeared in 6CC, and TCC corresponded to the carboxylate (COONa) groups. The peak was sharper for TCC than 6CC represents the higher carboxyl groups as compared to 6CC. The quantitative determination of carboxyl groups is determined by the conductometric titration, as explained in the next section. Interestingly, the peaks at 1739 cm^{-1}, 1460 cm^{-1}, 1240 $cm^{-1,}$ and 810 cm^{-1} due to hemicellulose and lignin have disappeared. The peak at 1515 cm^{-1} responsible for C=C aromatic symmetrical stretching in the lignin unit decreased in 6CC and completely disappeared in TCC. The FTIR spectra for each sample are a replica of 20 runs.

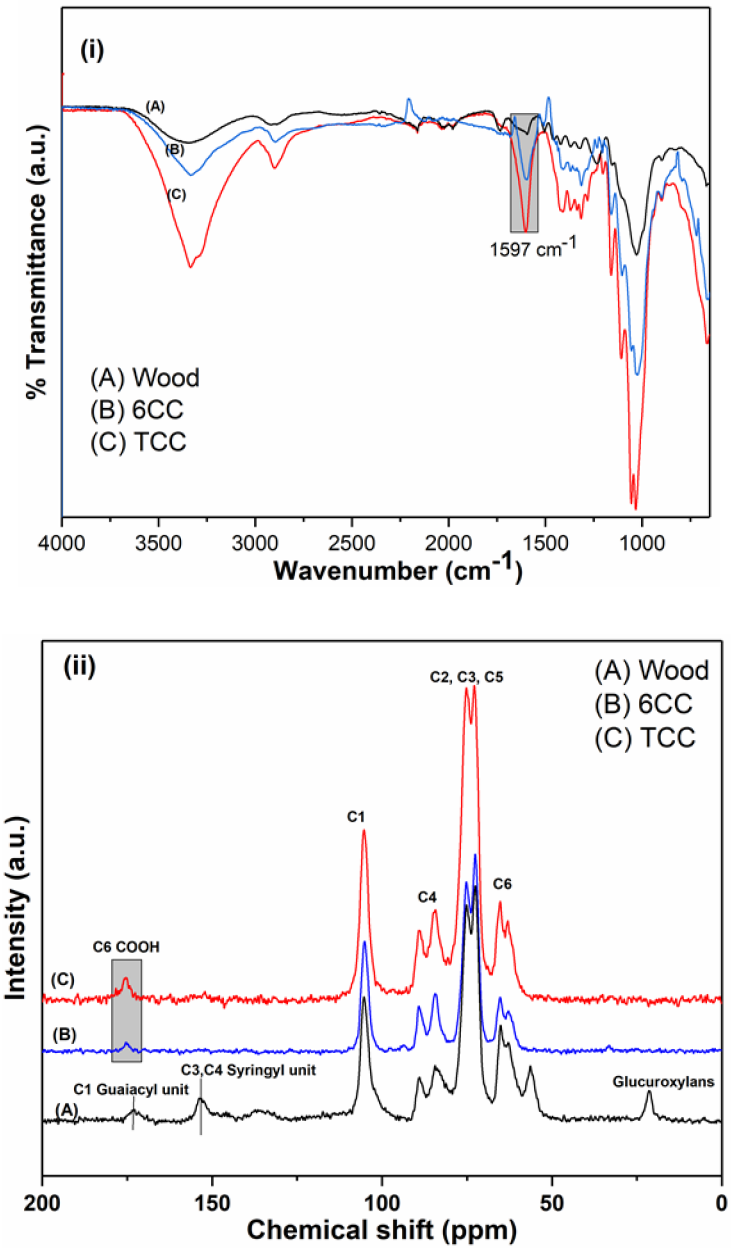

Figure 2. (**i**) FTIR of wood, 6CC and TCC; (**ii**) ^{13}C CPMAS NMR of wood, 6CC and TCC.

Conductometric titration curves for 6CC and TCC are presented in Figure S1 in Supplementary Information and were used to calculate the carboxylate content. The carboxylate content observed for 6CC was 0.64 mmol/g and TCC was 1.14 mmol/g. The results clearly indicate that TCC posses higher surfacial charges as compared to 6CC, which will lead to comparatively higher removal of Pb^{2+} ions from water.

The solid-state ^{13}C CPMAS NMR spectra of raw wood fibers, 6CC and TCC are presented in Figure 2ii. The area between 60–70 ppm represented C6 carbon of the primary alcohol group in the cellulose chain. Another group of peaks between 70–80 ppm was designated C2, C3, and C5 carbons, while the peaks appeared between 80–95 ppm associated with C4 carbon, and the peaks between 100–110 ppm corresponded to the anomeric carbon C1. The NMR spectra of raw wood fibers displayed discrete peaks at 21 and 56 ppm represent glucoroxylans of hemicellulose. Additionally, the peaks at 153 and 171–172 ppm belonged to C1 carbon of guaiacyl units and C4, C3 carbons of syringyl units of lignin. The loss of distinct lignin and hemicellulose peaks in NMR of 6CC and TCC confirms

the removal of hemicellulose and lignin during the oxidation processes. It was already evidenced that nitro-oxidation is very effective in removing lignin, hemicellulose, and other impurities from raw biomass [3].

WAXD patterns obtained from raw wood, 6CC and TCC are illustrated in Figure S2 in Supplementary Information. These patterns depict the presence of cellulose I structures in raw wood, 6CC and TCC, whereby the peaks appeared at 2θ of 16.4°, 22.5°, corresponding to the (110), and (200) reflection planes, respectively. The diffraction peak at 2θ of 34.9° due to (004) plane was present in wood and 6CC but disappeared in the TCC sample. Notably, the diffraction peaks related to the (110) and (102) planes of cellulose I structure did not appear in the WAXD patterns of raw wood, 6CC and TCC [37]. The disappearance of the (110) peak can be attributed to the presence of residual hemicellulose and lignin around the crystal structure of cellulose which disrupts the hydrogen bonding of the plane. The WAXD pattern in TCC showed the broad peaks rather than sharper peaks in WAXD pattern for wood and 6CC. This indicates that the crystallinity in TCC was highly decreased due to the introduction of carboxylate groups at C2, C3, C6 positions.

3.2. Morphological Characterization of 6CC and TCC

TEM images of 6CC and TCC obtained from raw wood fiber are shown in Figure 3. These images depict that the 6CC and TCC appeared in namometer size fibrous structure. In total 20 fibers were taken from the images to calculate the average (avg.) length (L) and width (W) of fibers using ImageJ software. It was found that 6CC possessed avg. L of 1044 ± 208 nm and avg. W = 6 ± 1.5 nm. While TCC fibers were in the range of avg. L of 750 ± 110 nm and avg. W of 4.5 + 1.8 nm. AFM images in Figure 4 were used to calculate the thickness of the fibers. In total 5–6 spots on different fibers of AFM image were considered to calculate the average thickness of the fibers. Based on that, the avg. thickness measured for 6CC and TCC was 1.69 and 1.23 nm, respectively.

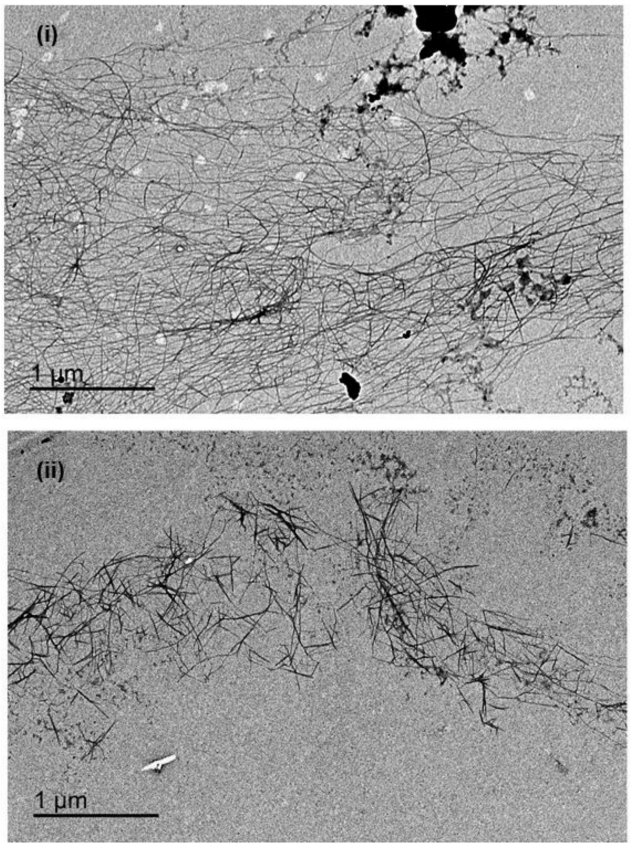

Figure 3. TEM of (**i**) 6CC and (**ii**) TCC.

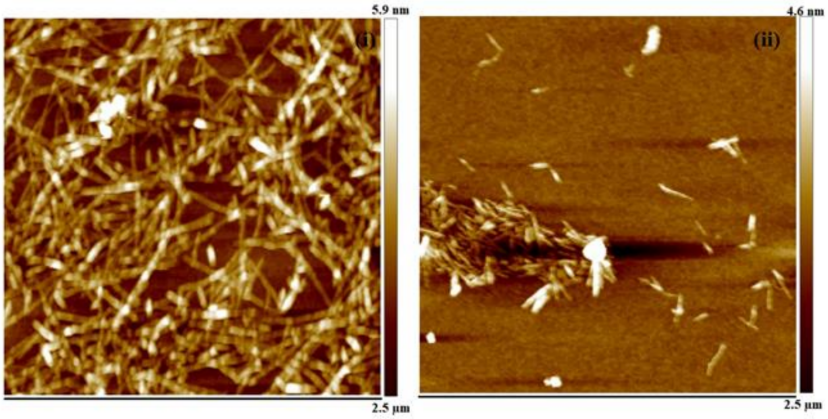

Figure 4. AFM images (**i**) 6CC and (**ii**) TCC.

3.3. Metal Ion Remediation of Pb^{2+} Contaminated Water by 6CC and TCC

Measured amounts (5 mL) of 6CC and TCC samples were introduced into water solutions that had been contaminated by Pb^{2+} metal ions. The 6CC and TCC nanofibers were introduced into solutions containing different concentrations of Pb^{2+}.

In Figure 5i, the photographs on the remediation of Pb^{2+} ions using 6CC are presented. It was noted that in most sample vials, a white powder could be seen settled at the bottom of the vials. We believe this white powder to be the Pb^{2+} ions that have been precipitated out on the introduction of the 6CC. In the samples containing 6CC nanofibers, a gelation effect is hardly seen in the samples containing Pb^{2+} ions. This is likely due to when the carboxycellulose has either less or equal carboxylate concentration to the concentration of the metal ions; the carboxycellulose nanofibers cannot fully adsorb the metal ions and allow them to precipitate out. This phenomenon does not occur in the TCC samples, and mostly gelation was seen in the vial. This further indicates that the TCC consist of higher carboxylate content that has allowed the Pb^{2+} ions to get adsorbed on its surface more efficiently.

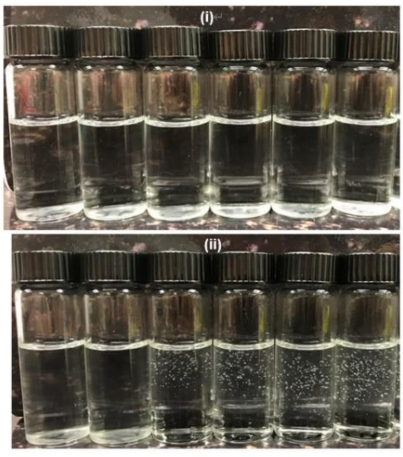

Figure 5. Photographs of remediation experiments (**i**) 5 mL of 0.02 wt% of 6CC mixed with 5 mL of varying concentration of Pb^{2+} (left to right: 5, 10, 25, 50, 100 and 250 ppm), (**ii**) 5 mL of 0.02 wt% of TCC mixed with 5 mL of varying concentration of Pb^{2+} (left to right: 5, 10, 25, 50, 100 and 250 ppm).

To confirm the removal efficiency of 6CC and TCC against Pb^{2+} ions, the FTIR of floc was performed as presented in Figure S3 in Supplementary Information. Here, a floc sample is referred to a sample containing adsorbed Pb^{2+} impurities on carboxycellulose nanofibers (6CC or TCC). The graph indicates a broad distinct peak of 1594 cm^{-1} in both 6CC and TCC floc representing the cross-linking of carboxylate groups of nanofibers and

Pb^{2+} ions, although this phenomenon was not clearly visible in the photographs presenting the remediation of Pb^{2+} ions using 6CC (Figure 5i).

The phenomenon of Pb^{2+} ion removal by nanofibers (6CC and TCC) in suspension is explained by SEM/EDS methods. SEM images of floc formed on adding Pb^{2+} (250 ppm) solution in nanofibers suspension is depicted in Figure 6i,iii. SEM images were taken after drying/coating the samples on Si wafer. As a result, the original morphology of nanofibers disappeared, and the sample appeared as a sheet. The floc of Pb^{2+}(250 ppm)@6CC appeared as a smoother surface as compared to Pb^{2+}(250 ppm)@TCC because of the longer fiber length in 6CC than TCC. In Figure 6iiii, a thick cloud of Pb^{2+} ions on the surface of the nanofibers can be seen, which confirms the precipitation of Pb impurities during the remediation process. The quantitative evidence of the presence of Pb^{2+} onto nanofibers surface was supported by EDS spectra, shown in Figure 6ii,iv. In corresponding EDS spectra, the Carbon (C), Oxygen (O), Sodium (Na) peaks represented carboxylate nanofibers, while Pb peak designated Pb^{2+} ions. The Pb peak was more prominent in TCC than 6CC, indicating the adsorption of more Pb^{2+} ions onto the TCC surface due to high carboxylate content.

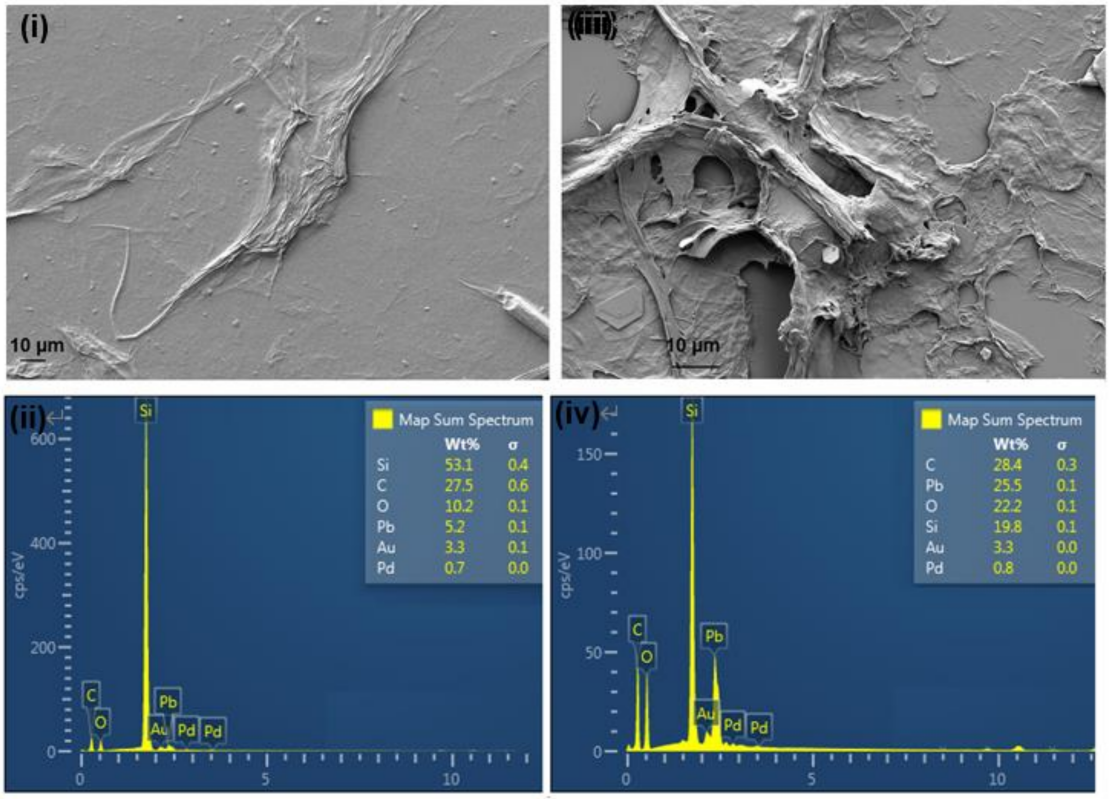

Figure 6. (**i**,**ii**) SEM images Pb^{2+}(250 ppm)@6CC and its corresponding EDX; (**iii**,**iv**) SEM image of Pb^{2+}(250 ppm) @TCC and its corresponding EDX.

The data obtained from ICP-MS was used to calculate the parameters to fit into Langmuir isotherm model. Table 1 demonstrates the calculations for measuring Qe (experimental adsorption capacity), Ce (concentration of Pb^{2+} used for the experiments). The ideal adsorption capacity for TCC was calculated based on the concentration of Pb^{2+} used in the solution to the concentration of TCC used for the experiments. Correspondingly, the adsorption efficiency of 6CC and TCC was calculated at different concentrations of Pb^{2+} ions. The removal efficiency of the 6CC and TCC nanofibers was between 77–99% when exposed to Pb^{2+} concentrations between 5 ppm and 250 ppm (Figure 7ii). The TCC showed a higher removal efficiency of 99% when the concentration of Pb^{2+} ions was 5 ppm, and this decreased to 78% when the Pb^{2+} concentration was 250 ppm. As compared to TCC, 6CC showed lower removal efficiency against Pb^{2+} ions. This can be explained by the

difference in the carboxylate content of 6CC and TCC. TCC exhibited carboxylate content of 1.14 mmol/g, and 6CC showed 0.64 mmol/g.

Table 1. Calculated Ideal Adsorption Capacity and Experimental Adsorption Capacity Against Pb^{2+} Ions by TCC.

Original Pb^{2+} Conc. before ICP-MS (ppm) Ce	Final Pb^{2+} from ICP-MS (ppb)	Original Pb^{2+} Conc. by ICPMS (ppb)	Adsorption Efficiency	Original Pb^{2+} Quantity (mg)	Original TCC- 0.02 wt% in 5mL (g)	Ideal Adsorption Capacity	Experimental Adsorption Capacity Qe
5	2.9	100	0.991	0.005	0.001	5	4.955
10	0.9	100	0.971	0.01	0.001	10	9.71
50	18	100	0.82	0.05	0.001	50	41
100	19	100	0.81	0.1	0.001	100	81
250	22	100	0.78	0.25	0.001	250	195

Adsorption efficiency = (original Pb^{2+} conc.—final Pb^{2+} conc.)/original Pb^{2+} conc. Ideal adsorption capacity = milligrams of Pb^{2+} in solution/grams of TCC in suspension. Experimental adsorption capacity = adsorption efficiency × ideal adsorption capacity. Qe = experimental adsorption capacity. Ce = original concentration of Pb^{2+} in ppm.

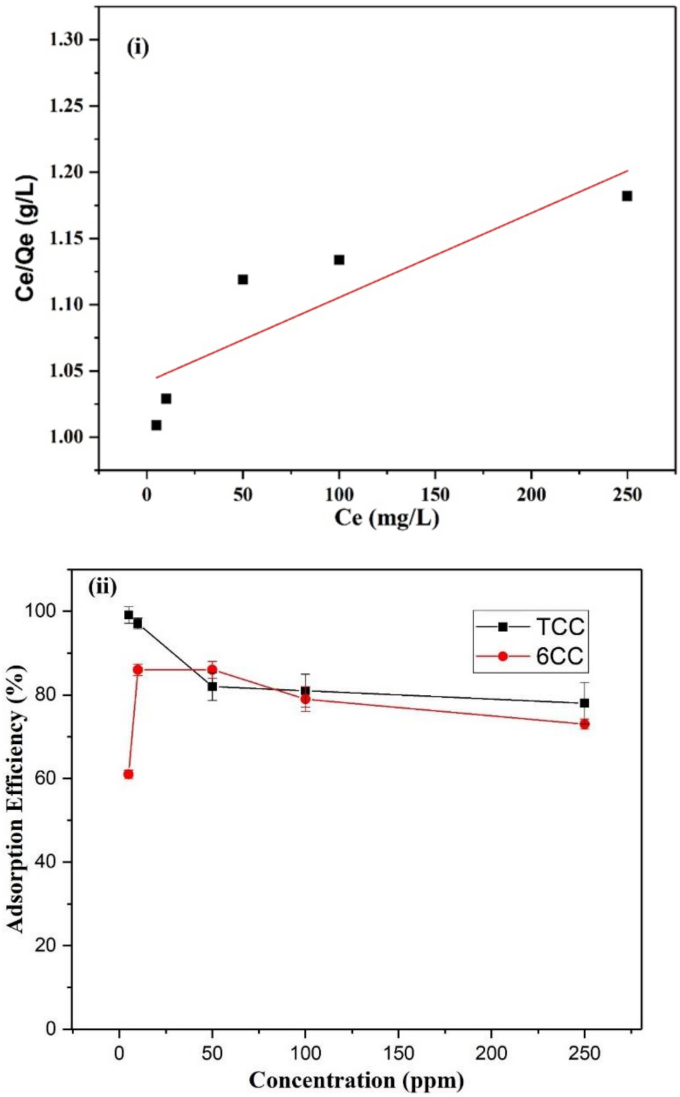

Figure 7. (**i**) Langmuir isotherm fitting for TCC; (**ii**) adsorption efficiency of 6CC and TCC.

Based on the Langmuir isotherm model, the coefficient of the LSRL of Ce against Ce/Qe is 6.37316E-4 as the reciprocal of the adsorption capacity. Thus, the adsorption capacity (Qm) obtained for TCC was 1569 mg/g with R^2 0.69531, showing conformity to the Langmuir isotherm model (Figure 7i).

A comparative table showing the maximum adsorption capacity (Qm) of the reported substrate in the literature and TCC is given in Table 2. It was interesting to note that the TCC demonstrated in this study is lower the maximum adsorption capacity of the most effective adsorbent reported to date, i.e., nitro-oxidized cellulose nanofibers (NOCNF) [9]. However, TCC has shown higher adsorption capacity than the reported organic substrate such as modified lignin [41], sago waste [42], thiol-, ethylenediamine- and diethylenediamine-modified cellulose nanofibers [43,44]. Lately, a nanocomposite system containing carboxymethylcellulose (CMC) and polyacrylic acid (PAA) was demonstrated, which exhibited very efficient Pb^{2+} ion removal of 900–952 mg/g, which is significantly lower than the TCC reported in this study. There have been several reports discussing the adsorption efficiency of biobased materials [45–47].

Table 2. Comparison of the Maximum Adsorption Capacity (Qm) Value Obtained from TCC with Different Types of Adsorbent Reported in the Literature.

Adsorbent	Maximum Adsorption Capacity (Qm) (mg/g)	References
TCC	1569	This study
NOCNF	2270	[9]
Flower-like magnesium oxide	1980	[48]
CMC-g-PAA	990	[49]
CMC-g-PAA/5% APT	952	[49]
Modified lignin	95.8	[41]
Sago waste	46.6	[42]
Sepiolite clay	93.4	[50]
Diethylemetriamine bacterial cellulose	31.4	[44]
Thiol modified CNF	131	[43]

TCC 2,3,6-tricarboxycellulose, CMC carboxymethyl cellulose, g grafted, PAA polyacrylic acid, APT attapulgite hydrogel, CNF cellulose nanofibers.

4. Conclusions

In this study, TCC with a high negative surface charge (1.14 mmol/g carboxylate content) was prepared using the three-step oxidation process, including nitro-oxidation, periodate oxidation and sodium chlorite oxidation. This is the first study to introduce raw wood in nitro-oxidation to produce 6CC. To obtain the high surface-charged substrate for Pb^{2+} ions removal, 6CC was further introduced to sequential oxidation. By doing so, the obtained TCC was of high carboxylate content (1.14 mmol/g) and low crystallinity, which has enabled it as an excellent substrate to remove Pb^{2+} ion impurities with a maximum removal efficiency of 1569 mg/g. Based on the evidence gathered from this study, it is proposed that the mechanism in which Pb^{2+} ions are removed from solution by TCC nanofibers is via adsorption and precipitation.

Supplementary Materials: The following are available online at https://www.mdpi.com/article/10.3390/polysaccharides2020017/s1, Figure S1: Coductometric titration for (i) 6CC, (ii) TCC, Figure S2: WAXD pattern for raw wood, 6CC and TCC, Figure S3: FTIR graph of floc consist of (i) Pb^{2+}(250 ppm)@ 6CC, (ii) Pb^{2+}(250 ppm)@ TCC, Figure S4: Scheme for preparation of TCC.

Author Contributions: Data curation, M.N. and W.L.; Formal analysis, S.K.S.; Funding acquisition, B.S.H.; Investigation, P.R.S. and S.K.S.; Methodology, M.N., W.L. and L.K.; Project administration, B.S.H.; Resources, B.S.H.; Supervision, P.R.S. and B.S.H.; Writing—original draft, P.R.S.; Writing—review & editing, P.R.S. and S.K.S. All authors have read and agreed to the published version of the manuscript.

Funding: The financial support for this work was provided by a grant from the Polymer Program of the Division of Materials Science in the National Science Foundation (DMR-1808690) and APC was funded by PRS collected vouchers.

Institutional Review Board Statement: Not applicable.

Informed Consent Statement: Not applicable.

Data Availability Statement: Not applicable.

Acknowledgments: The authors would like to thank Chung-Chueh Chang and Ya-Chen Chuang (ThINC facility at AERTC, Stony Brook University) for conducting TEM, AFM measurements, and Martin Ziliox (NMR facility at Stony Brook University) for the NMR analysis.

Conflicts of Interest: The authors declare no conflict of interest.

References

1. Moon, R.J.; Martini, A.; Nairn, J.; Simonsen, J.; Youngblood, J. Cellulose nanomaterials review: Structure, properties and nanocomposites. *Chem. Soc. Rev.* **2011**, *40*, 3941–3994. [CrossRef]
2. Kumar, R.; Singh, S.; Singh, O.V. Bioconversion of lignocellulosic biomass: Biochemical and molecular perspectives. *J. Ind. Microbiol. Biotechnol.* **2008**, *35*, 377–391. [CrossRef]
3. Sharma, P.R.; Joshi, R.; Sharma, S.K.; Hsiao, B.S. A Simple approach to prepare carboxycellulose nanofibers from untreated biomass. *Biomacromolecules* **2017**, *18*, 2333–2342. [CrossRef] [PubMed]
4. Chin, K.-M.; Ting, S.S.; Ong, H.L.; Omar, M. Surface functionalized nanocellulose as a veritable inclusionary material in contemporary bioinspired applications: A review. *J. Appl. Polym. Sci.* **2018**, *135*, 46065. [CrossRef]
5. Ogushi, Y.; Sakai, S.; Kawakami, K. Synthesis of enzymatically-gellable carboxymethylcellulose for biomedical applications. *J. Biosci. Bioeng.* **2007**, *104*, 30–33. [CrossRef] [PubMed]
6. Coseri, S.; Biliuta, G.; Simionescu, B.C.; Stana-Kleinschek, K.; Ribitsch, V.; Harabagiu, V. Oxidized cellulose—Survey of the most recent achievements. *Carbohydr. Polym.* **2013**, *93*, 207–215. [CrossRef]
7. Zhang, S.; Li, J.; Chen, S.; Zhang, X.; Ma, J.; He, J.J.C.P. Oxidized cellulose-based hemostatic materials. *Carbohydr. Polym.* **2020**, *230*, 115585. [CrossRef]
8. Sharma, P.R.; Chattopadhyay, A.; Sharma, S.K.; Geng, L.; Amiralian, N.; Martin, D.; Hsiao, B.S. Nanocellulose from spinifex as an effective adsorbent to remove cadmium (II) from water. *ACS Sustain. Chem. Eng.* **2018**, *6*, 3279–3290. [CrossRef]
9. Sharma, P.R.; Chattopadhyay, A.; Zhan, C.; Sharma, S.K.; Geng, L.; Hsiao, B.S. Lead removal from water using carboxycellulose nanofibers prepared by nitro-oxidation method. *Cellulose* **2018**, *25*, 1961–1973. [CrossRef]
10. Zhan, C.; Sharma, P.R.; Geng, L.; Sharma, S.K.; Wang, R.; Joshi, R.; Hsiao, B.S. Structural characterization of carboxyl cellulose nanofibers extracted from underutilized sources. *Sci. China Ser. E Technol. Sci.* **2019**, *62*, 971–981. [CrossRef]
11. Liang, L.; Bhagia, S.; Li, M.; Huang, C.; Ragauskas, A.J.J.C. Cross-linked nanocellulosic materials and their applications. *Chem. Sus. Chem.* **2020**, *13*, 78–87. [CrossRef]
12. Sharma, P.R.; Sharma, S.K.; Antoine, R.; Hsiao, B.S. Efficient removal of arsenic using zinc oxide nanocrystal-decorated regenerated microfibrillated cellulose scaffolds. *ACS Sustain. Chem. Eng.* **2019**, *7*, 6140–6151. [CrossRef]
13. Zhan, C. Structural Characterization of Nanocellulose-Based Composite Materials and Their Water Purification Applications. Ph.D. Thesis, State University of New York at Stony Brook, Stony Brook, NY, USA, 2019.
14. Qua, E.; Hornsby, P.; Sharma, H.S.; Lyons, G.; McCall, R. Preparation and characterization of poly (vinyl alcohol) nanocomposites made from cellulose nanofibers. *J. Appl. Polym. Sci.* **2009**, *113*, 2238–2247. [CrossRef]
15. Sharma, S.K.; Sharma, P.R.; Lin, S.; Chen, H.; Johnson, K.; Wang, R.; Borges, W.; Zhan, C.; Hsiao, B.S. Reinforcement of natural rubber latex using jute carboxycellulose nanofibers extracted using nitro-oxidation method. *Nanomaterials* **2020**, *10*, 706. [CrossRef]
16. Hu, J.; Li, H.-Y.; Williams, G.R.; Yang, H.-H.; Tao, L.; Zhu, L.-M. Electrospun poly (N-isopropylacrylamide)/ethyl cellulose nanofibers as thermoresponsive drug delivery systems. *J. Pharm. Sci.* **2016**, *105*, 1104–1112. [CrossRef]
17. Capezza, A.J.; Wu, Q.; Newson, W.R.; Olsson, R.T.; Espuche, E.; Johansson, E.; Hedenqvist, M.S. Superabsorbent and fully biobased protein foams with a natural cross-linker and cellulose nanofibers. *ACS Omega* **2019**, *4*, 18257–18267. [CrossRef]
18. Zhang, N.; Zang, G.-L.; Shi, C.; Yu, H.-Q.; Sheng, G.-P. A novel adsorbent TEMPO-mediated oxidized cellulose nanofibrils modified with PEI: Preparation, characterization, and application for Cu (II) removal. *J. Hazard. Mater.* **2016**, *316*, 11–18. [CrossRef] [PubMed]
19. Sharma, P.R.; Sharma, S.K.; Borges, W.; Chen, H.; Hsiao, B.S. Remediation of UO_2^{2+} from water by nitro-oxidized carboxycellulose nanofibers: Performance and mechanism. In *Contaminants in Our Water: Identification and Remediation Methods*; ACS Publications: Washington, DC, USA, 2020; pp. 269–283.
20. Saito, T.; Kimura, S.; Nishiyama, Y.; Isogai, A. Cellulose nanofibers prepared by TEMPO-mediated oxidation of native cellulose. *Biomacromolecules* **2007**, *8*, 2485–2491. [CrossRef]
21. Kim, U.-J.; Kuga, S.; Wada, M.; Okano, T.; Kondo, T. Periodate oxidation of crystalline cellulose. *Biomacromolecules* **2000**, *1*, 488–492. [CrossRef] [PubMed]
22. Varma, A.; Kulkarni, M.P. Oxidation of cellulose under controlled conditions. *Polym. Degrad. Stab.* **2002**, *77*, 25–27. [CrossRef]
23. Buslov, D.; Korolik, E.; Zhbankov, R.; Bashmakov, I.; Kaputskij, F. Spectroscopic study of tricarboxycellulose salts with Y 3+, Ba 2+, and Cu 2+ cations. *Vysokomol. Soedin. Ser. B* **1994**, *36*, 836–839.
24. Sharma, P.R.; Varma, A.J. Thermal stability of cellulose and their nanoparticles: Effect of incremental increases in carboxyl and aldehyde groups. *Carbohydr. Polym.* **2014**, *114*, 339–343. [CrossRef]
25. Mendoza, D.J.; Browne, C.; Raghuwanshi, V.S.; Simon, G.P.; Garnier, G. One-shot TEMPO-periodate oxidation of native cellulose. *Carbohydr. Polym.* **2019**, *226*, 115292. [CrossRef]

26. Garrett, Q.; Simmons, P.A.; Xu, S.; Vehige, J.; Zhao, Z.; Ehrmann, K.; Willcox, M. Carboxymethylcellulose binds to human corneal epithelial cells and is a modulator of corneal epithelial wound healing. *Investig. Ophthalmol. Vis.* **2007**, *48*, 1559–1567. [CrossRef]
27. Borisova, B.; Sánchez, A.; Jiménez-Falcao, S.; Martín, M.; Salazar, P.; Parrado, C.; Pingarrón, J.M.; Villalonga, R. Reduced graphene oxide-carboxymethylcellulose layered with platinum nanoparticles/PAMAM dendrimer/magnetic nanoparticles hybrids. Application to the preparation of enzyme electrochemical biosensors. *Sens. Actuators B Chem.* **2016**, *232*, 84–90. [CrossRef]
28. Voisin, H.; Bergström, L.; Liu, P.; Mathew, A.P. Nanocellulose-based materials for water purification. *Nanomaterials* **2017**, *7*, 57. [CrossRef]
29. Kumar, R.; Kumari, S.; Surah, S.S.; Rai, B.; Kumar, R.; Sirohi, S.; Kumar, G. A simple approach for the isolation of cellulose nanofibers from banana fibers. *Mater. Res. Express* **2019**, *6*, 105601. [CrossRef]
30. Sinha, T. Polymers in Medicine and Surgery: Cellulosic Systems. Ph.D. Thesis, Indian Institute of Technology Delhi, New Delhi, India, 1983.
31. Holmes, C.; Wrobel, J.S.; MacEachern, M.P.; Boles, B.R. Collagen-based wound dressings for the treatment of diabetes-related foot ulcers: A systematic review. *Diabetes Metab. Syndr. Obes.* **2013**, *6*, 17. [CrossRef]
32. Varma, A.J.; Sharma, P.R.; Sarkar, D. Synthesis of Nanostructured Carboxycelluloses from Non-Wood Cellulose. U.S. Patent US10,017,583, 10 July 2018.
33. Hoenich, N.A. Cellulose for medical applications: Past, present, and future. *BioResources* **2006**, *1*, 270–280. [CrossRef]
34. Eldor, R.; Raz, I.; Ben Yehuda, A.; Boulton, A. New and experimental approaches to treatment of diabetic foot ulcers: A comprehensive review of emerging treatment strategies. *Diabet. Med.* **2004**, *21*, 1161–1173. [CrossRef]
35. Abou-Zeid, R.E.; Dacrory, S.; Ali, K.A.; Kamel, S. Novel method of preparation of tricarboxylic cellulose nanofiber for efficient removal of heavy metal ions from aqueous solution. *Int. J. Biol. Macromol.* **2018**, *119*, 207–214. [CrossRef] [PubMed]
36. Sharma, P.R.; Kamble, S.; Sarkar, D.; Anand, A.; Varma, A.J. Shape and size engineered cellulosic nanomaterials as broad spectrum anti-microbial compounds. *Int. J. Biol. Macromol.* **2016**, *87*, 460–465. [CrossRef]
37. Sharma, P.R.; Rajamohanan, P.R.; Varma, A.J. Supramolecular transitions in native cellulose-I during progressive oxidation reaction leading to quasi-spherical nanoparticles of 6-carboxycellulose. *Carbohydr. Polym.* **2014**, *113*, 615–623. [CrossRef]
38. Sharma, P.R.; Varma, A. Functionalized celluloses and their nanoparticles: Morphology, thermal properties, and solubility studies. *Carbohydr. Polym.* **2014**, *104*, 135–142. [CrossRef]
39. Sharma, P.R.; Varma, A.J. Functional nanoparticles obtained from cellulose: Engineering the shape and size of 6-carboxycellulose. *Chem. Comm.* **2013**, *49*, 8818–8820. [CrossRef]
40. Wang, J.-W.; Kuo, Y.-M. Preparation of fructose-mediated (polyethylene glycol/chitosan) membrane and adsorption of heavy metal ions. *J. Appl. Polym. Sci.* **2007**, *105*, 1480–1489. [CrossRef]
41. Demirbas, A. Adsorption of lead and cadmium ions in aqueous solutions onto modified lignin from alkali glycerol delignication. *J. Hazard. Mater.* **2004**, *109*, 221–226. [CrossRef]
42. Quek, S.; Wase, D.; Forster, C. The use of sago waste for the sorption of lead and copper. *Water SA* **1998**, *24*, 251–256.
43. Yang, R.; Aubrecht, K.B.; Ma, H.; Wang, R.; Grubbs, R.B.; Hsiao, B.S.; Chu, B. Thiol-modified cellulose nanofibrous composite membranes for chromium (VI) and lead (II) adsorption. *Polymer* **2014**, *55*, 1167–1176. [CrossRef]
44. Shen, W.; Chen, S.; Shi, S.; Li, X.; Zhang, X.; Hu, W.; Wang, H. Adsorption of Cu (II) and Pb (II) onto diethylenetriamine-bacterial cellulose. *Carbohydr. Polym.* **2009**, *75*, 110–114. [CrossRef]
45. Tran, H.N.; Nguyen, H.C.; Woo, S.H.; Nguyen, T.V.; Vigneswaran, S.; Hosseini-Bandegharaei, A.; Rinklebe, J.; Kumar Sarmah, A.; Ivanets, A.; Dotto, G.L.; et al. Removal of various contaminants from water by renewable lignocellulose-derived biosorbents: A comprehensive and critical review. *Crit. Rev. Environ. Sci. Technol.* **2019**, *49*, 2155–2219. [CrossRef]
46. Krivoshapkin, P.V.; Ivanets, A.I.; Torlopov, M.A.; Mikhaylov, V.I.; Srivastava, V.; Sillanpää, M.; Prozorovich, V.G.; Kouznetsova, T.F.; Koshevaya, E.D.; Krivoshapkina, E.F. Nanochitin/manganese oxide-biodegradable hybrid sorbent for heavy metal ions. *Carbohydr. Polym.* **2019**, *210*, 135–143. [CrossRef]
47. Tomina, V.V.; Stolyarchuk, N.V.; Melnyk, I.V.; Zub, Y.L.; Kouznetsova, T.F.; Prozorovich, V.G.; Ivanets, A.I. Composite sorbents based on porous ceramic substrate and hybrid amino- and mercapto-silica materials for Ni(II) and Pb(II) ions removal. *Sep. Purif. Technol.* **2017**, *175*, 391–398. [CrossRef]
48. Cao, C.-Y.; Qu, J.; Wei, F.; Liu, H.; Song, W.-G. Superb adsorption capacity and mechanism of flowerlike magnesium oxide nanostructures for lead and cadmium ions. *ACS Appl. Mater. Interfaces* **2012**, *4*, 4283–4287. [CrossRef]
49. Liu, J.; Si, J.; Zhang, Q.; Zheng, J.; Han, C.; Shao, G. Preparation of negatively charged hybrid adsorbents and their applications for Pb2+ removal. *Ind. Eng. Chem. Res.* **2011**, *50*, 8645–8657. [CrossRef]
50. Bektaş, N.; Ağım, B.A.; Kara, S. Kinetic and equilibrium studies in removing lead ions from aqueous solutions by natural sepiolite. *J. Hazard. Mater.* **2004**, *112*, 115–122. [CrossRef]